How does the protein environment optimize the thermodynamics of thiol sulfenylation? Insights from model systems to QM/MM calculations on human 2-Cys peroxiredoxin.

Julianna Oláh[a], *, Laura A. H. van Bergen[b], Frank De Proft[c], Goedele Roos[d]

* [a]Corresponding author: Dr. Julianna Oláh
Department of Inorganic and Analytical Chemistry, Budapest University of Technology and Economics
H-1111 Budapest, Gellért tér 4. Hungary
tel: (00)36/1-4632278
julianna.olah@mail.bme.hu

[b] Laura A. H. van Bergen
General Chemistry, Vrije Universiteit Brussel
Pleinlaan 2, 1050 Brussels, Belgium.
Phone:0032-2-6293673
lvbergen@vub.ac.be

[c] Prof. Frank De Proft
General Chemistry, Vrije Universiteit Brussel
Pleinlaan 2, 1050 Brussels, Belgium.
Phone:0032-2-6293310
fdeprof@vub.ac.be

* [d] Corresponding author: Dr.Goedele Roos
General Chemistry, Vrije Universiteit Brussel, 1050 Brussels, Belgium
Structural Biology Brussels, VIB and Vrije Universiteit Brussel, 1050 Brussels, Belgium, 1050 Brussels, Belgium
Pleinlaan 2, 1050 Brussels, Belgium
Phone:0032-2-6293312
groos@vub.ac.be

Running title: Peroxiredoxin's thiol sulfenylation thermodynamics

Abstract

Protein thiol/sulfenic acid oxidation potentials provide a tool to select specific oxidation agents, but are experimentally difficult to obtain. Here, insights into the thiol sulfenylation thermodynamics is obtained from model calculations on small systems and from a quantum mechanics/molecular mechanics (QM/MM) analysis on human 2-Cys peroxiredoxin thioredoxin peroxidase B (Tpx-B). To study thiol sulfenylation in Tpx-B, our recently developed computational method to determine reduction potentials relatively compared to a reference system and based on reaction energies (REE) is updated. Tpx-B forms a sulfenic acid ($R\text{-}SO^-$) on one of its active site cysteines during reactive oxygen scavenging. The observed effect of the conserved active site residues is consistent with the observed hydrogen bond interactions in the QM/MM optimized Tpx-B structures and with free energy calculations on small model systems. The ligand effect could be linked to the complexation energies of ligand L with CH_3S^- and CH_3SO^-. Compared to QM only calculations on Tpx-B's active site, the QM/MM calculations give an improved understanding of sulfenylation thermodynamics by showing that other residues from the protein environment other than the active site residues can play an important role.

Keywords

redox chemistry, sulfenylation, peroxiredoxin, ligand effect, QM/MM

List of abbreviations

Prx: peroxiredoxin

QM/MM: quantum mechanics/molecular mechanics

TpxB: human 2-Cys peroxiredoxin thioredoxin peroxidase B

REE: Reduction potential from Electronic Energies

Introduction

Peroxiredoxins (Prxs) are essential anti-oxidant proteins defending the cell against oxidative stress. Prxs reduce reactive oxygen species (ROS) through a cysteine-based reaction mechanism [1]: during reactive oxygen scavenging, the active site cysteine (often referred to as peroxidatic cysteine Cys_P) is oxidized to sulfenic acid (Cys_P-OH) [2].

Sulfenic acid formation, also called sulfenylation, has long been regarded as a harmful cysteine modification, but is nowadays known as an intermediate in the redox regulation of signaling pathways[3], and in *de novo* disulfide bond formation [4]. The kinetic aspects of sulfenic acid formation are well documented in both Prx and low molecular weight thiols [5]. Rate constants depend on the thiol and on the oxidant, for example, with H_2O_2 as an oxidant, the rate constant varies between 1 $M^{-1}s^{-1}$ (for gluthation, GSH) and 10^8 $M^{-1}s^{-1}$ (for Prx) at pH 7.4-7.6 and 37 °C [6]; with GSH as thiol, the rate constants range between 10^2 $M^{-1}s^{-1}$ (for peroxynitrite) and 10^{10} $M^{-1}s^{-1}$ (for hydroxyl radicals) at pH 7.4 [4].

Experimental work can give insight into reaction rates of thiol sulfenylation reactions and can as such provide information on activation barriers, but the thermodynamic aspects and thus the equilibrium constants are running behind. Experimentally determined enzymatic catalyzed and non-catalyzed reduction potentials for thiol sulfenylation are not available, presumably due to the highly reactive nature of sulfenic acids [7] and high reaction rates between thiols and oxidants [5a]. Here we reveal the thermodynamics of thiol sulfenylation in human 2-cysteine peroxiredoxin thioredoxin peroxidase B (Tpx-B) via a combined quantum mechanics/molecular mechanics (QM/MM) analysis. To this end, our recently developed computational method to determine reduction potentials relatively compared to a reference system and based on reaction energies (REE)[8] is updated. The REE method was originally developed using substituted thiols and is now updated using a different set of model systems, namely CH_3SO^-*n*L/CH_3S^---*n*L systems with *n* the number and L the ligand, resembling better the active site of the enzyme (Scheme 1).

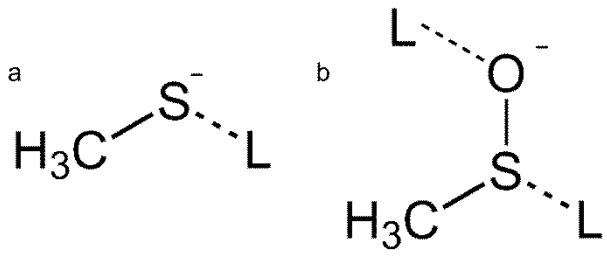

Scheme 1: a) CH_3S^---*n*L complex with *n* =1 and Ligand L b) L can interact with the oxygen atom or sulfur atom of CH_3SO^-

Our methodology is generally applicable to other systems and can provide insight into how the enzymatic environment contributes to the driving force of catalysis. Via this study, a complete picture of the energy-reaction coordinate diagram of thiol sulfenylation will be obtained. The relative reactivity of thiol-based peroxidases is presumably determined by kinetic factors, since the thermodynamic force for peroxide reduction is highly favorable[5a, 9]. However, studying the thermodynamic aspects of thiol sulfenylation is of fundamental importance since it determines the stability of the formed sulfenic acid. In addition, it could give us a better understanding of the direction of the electron flow and thus of the players of an electron transfer pathway.

We will focus on the 2-cysteine peroxiredoxin thioredoxin peroxidase B (Tpx-B) from human erythrocytes. Human Tpx-B is an obligate homodimer whose active site consists of Cys_P (Cys51) and of the highly conserved polar (Tyr43, Thr48, Glu54, Arg127 and Arg150), and non-polar residues (Pro44, Val50 and Trp86) [10] (Figure 1).

Figure 1: A Human peroxiredoxin Tpx-B is an obligate homodimer. **B** Conserved active site around Cys51. Figure generated from the X-ray structure with PDB ID: 1QMV with Pymol [11].

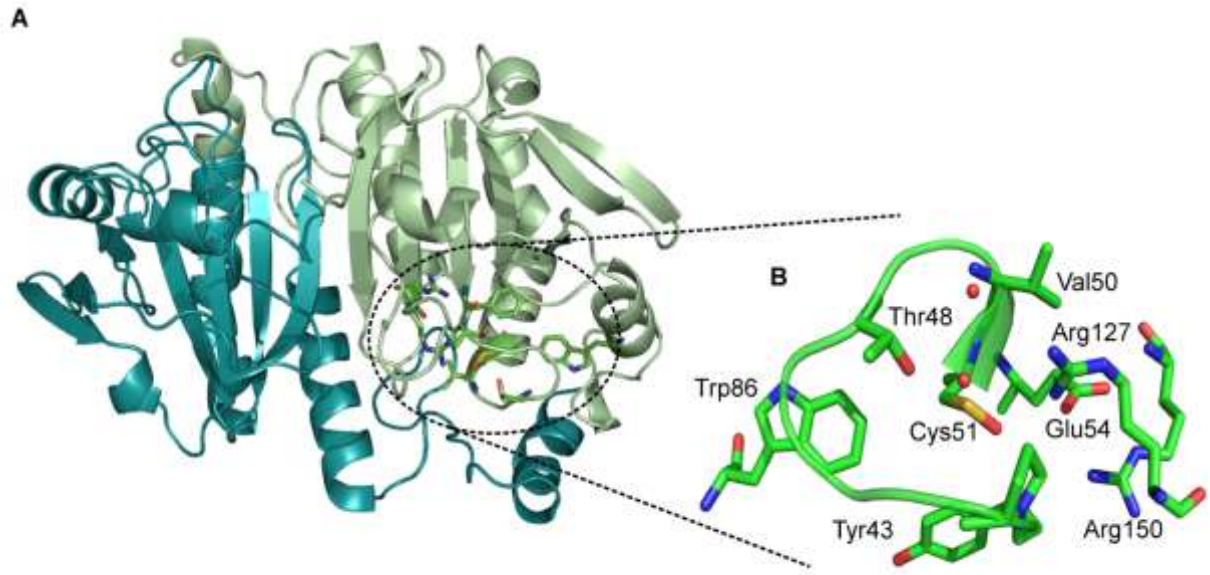

Arg127 was shown to have a crucial role in the reaction kinetics of human Prx oxidation with H_2O_2. The second order rate constant for the oxidation reaction of the human Prx mutant Arg127Lys with H_2O_2 was found to be 5 orders of magnitude lower compared to the WT [12]. In tryparedoxin peroxidase of *Leishmania donovani* [13], the active site Thr49Ala mutation was shown to decrease the oxidation rate with 2 orders of magnitude. A 60-90% drop of oxidation rate was found for the active site Thr107Ala mutation in peroxiredoxin Q of *Arabidopsis thaliana* [14]. The role of the conserved non-polar residues is still unknown. Their possible importance in thermodynamic aspects will be unraveled in this work.

Via a generally applicable computational protocol, insight is given into how the different elements of the enzymatic environment work together to optimize the sulfenylation thermodynamics. The thermodynamic determinants will be discussed in the light of kinetic

data, and given the high degree of conservation of the active site of human Prx2[10], our obtained results can be extended to other peroxiredoxins. Furthermore, calculations on model systems will shed light onto the general effects of polar and non-polar residues on thiol sulfenylation thermodynamics. Structural details will be discussed in the light of the thermodynamic data, by which structure and reactivity can be related.

Materials and Methods

Model systems

The structures of the following model systems: CH_3SO^-*n*L/CH_3S^---*n*L with *n*L= *1*CH_4, *1*C_2H_2, *1*H_2O, *1*NH_3, *1*CH_3COOH, *1*CH_3OH, *1*CH_3CONH_2, *2* CH_4, *2* C_2H_2, (Scheme 1) - for the $-SO^-$ form with L = CH_4, CH_3CONH_2 two conformations are considered: L interacts with the oxygen atom or sulfur atom of CH_3SO^- - are optimized in gas phase at the B3LYP/6-31+G(d,p) level. Frequency calculations were performed to check if the geometry is a minimum. Free energies in solution were calculated via a thermodynamic cycle[15]:

$$G^\circ(\varepsilon) = G^\circ_{gas} + \Delta G^\circ_{solv} + RT\ln(\frac{RT}{P}) \qquad (1)$$

with G°_{gas} the free energy in gas phase (standard state 1 atm) and ΔG°_{solv} the solvation free energy (standard state 1 mol/l). The $RT\ln(\frac{RT}{P})$ term makes the conversion between the gas phase standard state and the solution phase standard state. Free energies of solvation were calculated using the polarized continuum solvent model (PCM) [16], with UAHF radii and ε= 4, 10 and 20 at the HF/6-31+G(d) level[15b, 17]. Energy calculations were performed at the B3LYP/6-31+G(d,p) level using the PCM model [16], with UAHF radii and ε= 4, 10 and 20. All calculations were performed with Gaussian 03[18].

To generate Table 1, the structures of the model systems (plus one additional model system with L=Na^+) are also optimized at the MP2/6-31+G(d,p) and MP2/6-311++G(d,p) level with Gaussian03 [18] and at the M06-2X/6-31+G(d,p) level with Gaussian09 [19]. Free energies in solution are calculated via the same methodology as described in the previous paragraph.

Human PrxTpx-B

A small system of the active site around Cys_P (Cys51) of human Prx Tpx-B is built based on the X-ray coordinates 1QMV[10]. The model consists of Cys51 surrounded by Tyr43, Pro44, Thr48, Val50, Arg127 and a water molecule. Next to the WT system, the Val50Ala, the Tyr43Ala, the Thr48Ala and the Arg127Ala mutants were made. Hydrogen atoms were placed and optimized together with the side chain of Cys51 in its thiolate ($-S^-$) and sulfenic acid ($-SO^-$) forms at the B3LYP/6-31G(d) level using Gaussian 09[19]. Subsequent energy

calculations were performed at the B3LYP/6-31+G(d,p) level in a PCM solvent model [16] with UAHF radii and ε=4, using Gaussian03[18].

System setup, MD simulations and QM/MM calculations **Studied systems.** The 1QMV [10] crystal structure has been used for the modeling for the wild type Val50Ala, the Tyr43Ala, the Thr48Ala and the Arg127Ala mutants. System-setup, MM calculations and MD simulations, QM/MM calculations were carried out in exactly the same way for all systems. Furthermore, all systems were modeled separately, starting from system setup, both in the S- and SO- states of the Cystein 51, thus the following protocol was independently carried out for all systems.

System setup, MM and MD simulations In the calculations Chains A and B of the X-Ray structure 1QMV were used, as the two chains together form the active dimeric form of the protein. Hydrogen atoms were added to the initial X-Ray structure and their positions were optimized. The protonation states of acid and basic residues were predicted by using the PROPKA program[20] and all titratable residues were modeled in the natural protonation states. The hydrogen-bonding environment of all histidine residues was checked and all of them were modeled as δ-protonated. The Sγ sulfur atom of Cys51 of Chain A was used as the centre of the system. The structures were solvated within a 60 Å box with 8000 pre-equilibrated water molecules, represented by the TIP3P model, centered on the Sγ sulfur of Cys 51 (Chain A). Water molecules farther than 25 Å from the Sγ sulfur of Cys 51 (Chain A) were removed. The added water was then equilibrated by stochastic boundary MD at 300 K over 20 ps with respect to the protein structure and minimized. Then, all atoms within a 25 Å sphere around Sγ sulfur of Cys 51 (Chain A) were minimized, followed by stochastic boundary MD simulation of the whole system. Atoms farther than 25 Å from the Sγ sulfur of Cys 51 (Chain A) were fixed throughout the simulations. Earlier results on highly charged systems indicated that fixing of atoms farther than 25 Å than the centre of the system might be preferred to artificial truncation of the system [21]. All systems were heated to 300 K over 60 ps followed by a 300 ps long equilibration of the system. Subsequent MD equilibrations at 300 K were carried out over 5000 ps. The CHARMM27 force field[22] has been used for protein and water molecules, while the capping N-terminal N-carbamoyl-alanine (NCB) residue was described by a custom CHARMM topology file, for which atom typing and assignment of parameters and charges were carried out by analogy. Details of topology file and of the parameters of NCB can be found in the supporting information. All modeling calculations were carried out using the CHARMM software package [23].

The S^- and SO^- forms of cysteine were created using patch residues which are included in the supporting information. Parameters for the S- form were previously published[24], while the SO- containing residue was parameterized using ethyl-SO- using the charmm 27 parameter assigning protocol. Unfortunately, for such system the recently developed CHARMM General Force Field (CGenFF)[25] was not applicable. Details of the used parameters are also included in the SI.

Estimation of the reduction potentials from QM/MM snapshots Every 400 ps a snapshot has been taken from the trajectory file of each MD simulation run and thorough QM/MM optimization of the structure was carried out using the Chemshell software[26] with Gaussian 09 as the QM code. The QM region of the calculation was exactly the same system as in the QM only calculations, described above in order to assure maximal comparability between them. In every case care was taken to cut only non-polar C-C bonds in order to minimize unrealistic effects arising from cutting polar bonds. Using the coupling=shift option, the charges of MM atoms bonded to QM atoms were set to zero and redistributed onto the neighboring MM atoms. Extra charges were added by default to compensate for the dipole created by this shift. All atoms within a 12 Å-sphere of the Sγ atom of Cys51 (Chain A) were MM or QM optimized, the positions of all atoms outside this sphere were kept fixed. After QM/MM optimization of the system, a single point calculation on the QM-region was carried out at the B3LYP/6-31+G(d,p) level in a PCM solvent model [16] with UAHF radii and ε=4, using Gaussian03[18]. This procedure was strongly preferred to comparing QM/MM energies of the optimized structures, as the QM/MM energy of the system strongly depends both on the MM contribution to the energy and on the interaction between the QM and MM regions, making direct comparison impossible for the various snapshots.

Results and discussion

Reduction potentials from Electronic Energies: the REE method updated

The Reduction potential from Electronic Energies (REE) method was recently introduced to calculate thiol sulfenylation reduction potentials on large systems [8]. In a series of analogous reactions, the non-electronic contributions to the reaction free energy are constant and as such, the electronic part of the reaction free energy (which is the reaction energy) correlates with the reaction free energy. Therefore, the calculated energy differences (ΔE) can be linked to free energy differences ($\Delta G°'$). This method was developed using substituted thiols [8] and is now updated using a different set of model systems, resembling better the enzyme's active site. CH_3SO^-*n*L/CH_3S^---*n*L with *n*L= *1*CH_4, *1*C_2H_2, *1*H_2O, *1*NH_3, *1*CH_3COOH, *1*CH_3OH, *1*CH_3CONH_2, *2* CH_4, *2* C_2H_2, are used as model system (Scheme 1). For the -SO^- form with L = CH_4, CH_3CONH_2 two conformations are considered: L interacts with the oxygen atom or sulfur atom of CH_3SO^- (Scheme 1).

The RS^- oxidation mediated by H_2O_2 is given by the following reaction:

$$CH_3S^-\text{--}n\text{L}\ (\varepsilon) + H_2O_2 \rightarrow CH_3SO^-\text{--}n\text{L}\ (\varepsilon) + H_2O \qquad (2)$$

with ε the dilecetric consntant of the (enzymatic) environment.

Redox potentials are traditionally calculated for reduction processes and thus we associate $\Delta G°'(RSO^- / RS^-)$ and $\Delta E(RSO^- / RS^-)$ to the following reduction reaction (2), which corresponds to the reverse of the half-equation of reaction (2):

$$CH_3SO^-\text{--}n\text{L}\ (\varepsilon) + 2H^+\ (aq) + 2e^- \rightarrow CH_3S^-\text{--}n\text{L}\ (\varepsilon) + 2H_2O \qquad (3)$$

The second half-equation, also written for the reduction process, then reads:

$$H_2O_2 + 2H^+\ (aq) + 2e^- \rightarrow 2H_2O \qquad (4)$$

$\Delta G°'(RSO^- / RS^-)$ and $\Delta E(RSO^- / RS^-)$ are given by:

$$\Delta G°'(RSO^- / RS^-) = G°(RS^-) - G°(RSO^-) \quad (5)$$

$$\Delta E(RSO^- / RS^-) = E(RS^-) - E(RSO^-) \quad (6)$$

$G°(H_2O)$, $G°(H^+)$ and $-RT\ln 10^{-7}$, making the conversion between the standard state of 1 M H^+ (pH=0) and pH=7, are included as constant contributions in $\Delta G°'(RSO^- / RS^-)$. $G°(RS^-)$ and $G°(RSO^-)$ are the free energies in solvent for the solution standard state of 1 mol/l and are calculated via Eq. (6), as described, as the sum of the gas phase Gibbs free energy $G°_{gas}$ and the free energies of solvation $\Delta G°_{solv}$ of the oxidized and reduced forms [8, 15b, 17]:

$$\Delta G° = G°_{gas}(RS^-) - G°_{gas}(RSO^-) + \Delta G°_{solv,RS^-} - \Delta G°_{solv,RSO^-} + (p-r)RT\ln\frac{RT}{P} \quad (7)$$

p and r are the amounts of products and reactants and the $RT\ln(\frac{RT}{P})$ term makes the conversion between the gas phase standard state of 1 atm and the solution phase standard state of 1 mol/l. Note that for reaction (3), $p = r$ and thus, the $RT\ln(\frac{RT}{P})$ term vanishes here.

A correlation between $\Delta G°'(RSO^- / RS^-)$ and the energy $\Delta E(RSO^- / RS^-)$ for the CH_3SO^- *n*L/CH_3S^---*n*L reduction is found (Figure 2):

$$\Delta G°'(RSO^- / RS^-) = C\Delta E(RSO^- / RS^-) + B \quad (8)$$

with *C* the slope and *B* the intercept.

Figure 2: Correlation between the reaction free energy ($\Delta G°'(RSO^- / RS^-)$) and the reaction energy ($\Delta E(RSO^- / RS^-)$) of the sulfenic acid/thiol reduction reaction.

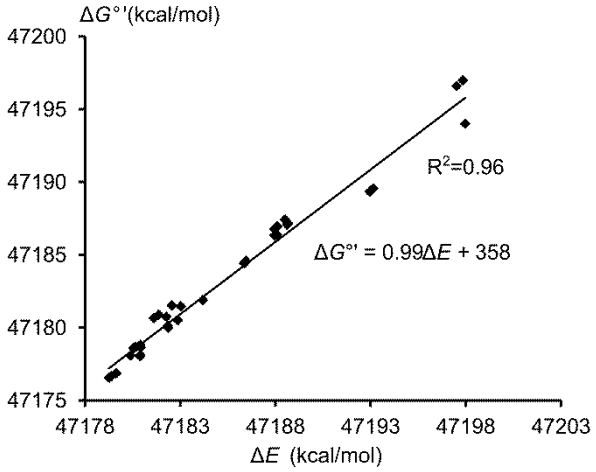

For human Tpx-B, the effect of several active site mutants will be calculated relative to wild type (WT):

$$\Delta\Delta G°'(RSO^- / RS^-)_{\text{mutant-WT}} = C\Delta E(RSO^- / RS^-)_{\text{WT}} - C\Delta E(RSO^- / RS^-)_{\text{mutant}} \quad (9)$$

with C = 0.99 obtained from the slope of the linear correlation found in Figure 2.

The Nernst equation can be used to convert differences in $\Delta G°'(RSO^- / RS^-)$ to reduction potential differences assuming that the reduction potential associated to reaction (4) is the same for the mutant and WT systems:

$$\Delta E°'_{\text{WT-mutant}} = -\frac{\Delta\Delta G°'(RSO^- / RS^-)_{\text{WT-mutant}}}{nF} \quad (10)$$

with n the number of transferred electrons (here 2) and F the Faraday constant.

Factors that control the thiolate oxidation: insights from calculations on CH_3SO^---nL/CH_3S^---nL model systems

Based on the structural arrangements in the X-ray structure 1QMV[10] of human Prx Tpx-B, small model complexes CH_3SO^---*n*L/CH_3S^---*n*L (scheme 1) are designed to give insight into the influence of polar and non-polar ligands on the thiol sulfenylation reduction potential. In the case of these small models, $\Delta G°'(RSO^- / RS^-)$ (Eq.(5)) can be calculated directly (Table 1). Table 1 shows the relative effect of polar and non-polar ligands on the free reaction energy calculated as $\Delta\Delta G°'(RSO^- / RS^-)_{ref-ligand} = \Delta G°'_{ref} - \Delta G°'_{ligand}$. Different theoretical methods to obtain this quantity (MP2, M06, B3LYP) show similar trends.

The most important trend obtained from these calculations is that $\Delta G°'(RSO^- / RS^-)$ increases in the presence of polar ligands and decreases in the presence of non-polar ligands, when the ligand interacts with the oxygen atom of the sulfenic acid $-SO^-$ (Scheme 1). This means that polar ligands thermodynamically favor the CH_3S^- oxidation when they interact with the oxygen atom of CH_3SO^-, while non-polar ligands disfavor sulfenylation. The cation Na^+ disfavors sulfenylation by ~2kcal/mol. The effect of the ligands interacting with the sulfur atom of the sulfenic acid form could only be assessed in two cases since most of the ligands placed in interaction with the sulfur atom of sulfenic acid redirects to the oxygen atom during the optimization procedure. Here, the results indicate that polar ligands decrease $\Delta G°'(RSO^- / RS^-)$, while non-polar ligands do not have a significant effect when they interact with the sulfur atom of the sulfenic acid.

The thermodynamic cycle depicted in Scheme 2 shows that $\Delta\Delta G°'(RSO^- / RS^-)_{ref-ligand}$ can be linked to the free energy changes upon ligand coordination (ligand taken in a general sense as the complete surrounding environment around CH_3S^- or CH_3SO^-) to the CH_3S^- and CH_3SO^- systems.

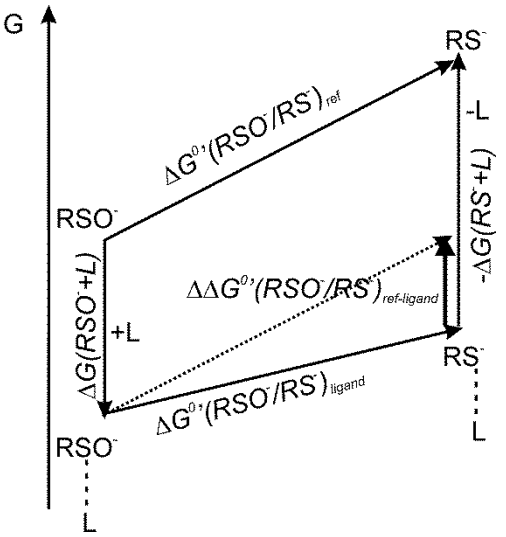

Scheme2: Thermodynamic cycle depicting the relationship between complexation energies of any ligand L with the CH_3S^- and CH_3SO^- systems and the $\Delta G^{\circ\prime}(RSO^- / RS^-)$ value.

Based on the cycle in Scheme 2, $\Delta\Delta G^{\circ\prime}(RSO^- / RS^-)_{ref-ligand}$ could also be calculated as the difference between the interaction energies of the CH_3S^- and CH_3SO^- systems with ligand L (eq.(10)) (See Supporting Information Table S1 for interaction energies of some ligands from Table 1). Therefore the calculated $\Delta\Delta G^{\circ\prime}(RSO^- / RS^-)_{ref-ligand}$ value could be interpreted as the differential stabilization of the CH_3SO^- and CH_3S^- systems by the ligand.

$$\Delta\Delta G^{\circ\prime}(RSO^- / RS^-)_{ref-ligand} = \Delta G^{\circ\prime}(RSO^- + L) - \Delta G^{\circ\prime}(RS^- + L) \quad (11)$$

Those ligands which interact more strongly with the CH_3SO^- system than with the CH_3S^- system will be characterized by a more negative $\Delta\Delta G^{\circ\prime}(RSO^- / RS^-)_{ref-ligand}$ value and will favor sulfenylation (like H_2O, see Table 1 and Supporting Information Table S1). Ligands interacting more strongly with the CH_3S^- system than with the CH_3SO^- system will lead to positive $\Delta\Delta G^{\circ\prime}(RSO^- / RS^-)_{ref-ligand}$ values therefore disfavor sulfenylation (like CH3COOH, Table 1 and Supporting Information Table S1). If the ligand interacts equally well with both CH_3S^- and CH_3SO^-, one obtains the same reduction potential as the reference system. Ligands may interact with CH_3SO^- on both the S and the O site of the molecule, leading to different interaction energies and thus to different $\Delta\Delta G^{\circ\prime}(RSO^- / RS^-)_{ref-ligand}$ values.

The fact that non-polar ligands hardly change the $\Delta G^{\circ\prime}(RSO^- / RS^-)$ when interacting with the sulfur atom of the sulfenic acid might be explained by the fact that the sulfur atom of both

RS^- and RSO^- similarly polarize the ligand, allowing the ligand to interact equally strongly with RS^- and RSO^-. An example is CH_4 interacting with the sulfur atom of the RSO^- (see Supporting Information table S1). However, when the non-polar ligand CH_4 interacts with the oxygen atom of the sulfenic acid, this oxygen atom can polarize the non-polar ligand to a different extent than RS^- allowing the ligand to interact more strongly with RS^- by which sulfenylation is disfavored (Table S1).

The cationic ligands Na^+ disfavors sulfenylation by about 2 kcal/mol. This result means that Na^+ interact more strongly with the sulfide form than with the sulfenic acid. Furthermore this result is consistent with the observed charge transfer from the anion to the cation (the Mulliken charge calculated at the B3LYP/6-31+G(d,p) level on the S atom in $CH3S^-$ without a ligand present is -0.92, while it is -0.51 when Na^+ is present) thereby decreasing the charge on the sulfide group, which as a consequence will be less likely to undergo oxidation than the reference system.

Factors that control the Cys51 oxidation in human Prx: results from QM calculations on a model of the active site around Cys51

From the X-ray structure of human Tpx-B (1QMV)[10], a model of the active site around Cys51 was built consisting of Tyr43, Pro44, Thr48, Val50, Arg127 and a water molecule (Figure 1, 3 and Methods section). For convenience, these structures will be called the QM models throughout the following discussion. After geometry optimization of the reduced ($Cys51\text{-}S^-$) and the oxidized ($Cys51\text{-}SO^-$) forms, hydrogen bonds between $Cys51\text{-}S^-$ and $Cys51\text{-}SO^-$ with the surrounding enzymatic environment could be identified (Figure 3, Table 2).

Figure 3: Interactions between Cys51-S^- (**A**) and Cys51-SO^- (**B**) in the QM optimized structures of Tpx-B. Color code: nitrogen: blue; oxygen: red; hydrogen: white; carbon: gray, sulfur: yellow. See Table 3 for the interaction distances.

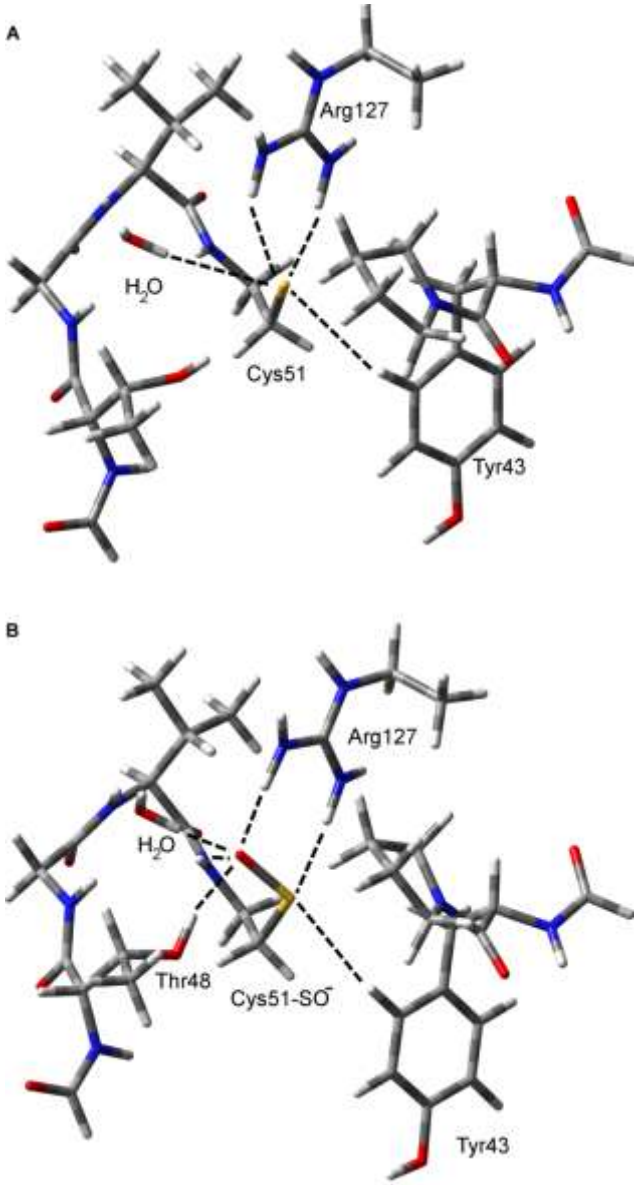

In the wild type (WT) structure, four hydrogen bonds with Cys51-S^- and five with Cys51-SO^- are found. These hydrogen bonds decrease the Cys51 p*K*a from 8.3 (p*K*a of free cysteine thiol)[27] to 5.7 and support as such the kinetically favored deprotonated –S^-/–SO^- oxidation

[5a]. The p*K*a was calculated in the reduced model system via the natural population analysis charge-p*K*a correlation method presented elsewhere [28]. The RSOH p*K*a is expected to be lower than the pK_a of the corresponding thiol [4]. In aqueous solution, the p*K*a for the sulfenyl group of CysOH is found to be between 6 and 10 [29]. Since the sulfenic acid pK_a is determined to be 6.1 in *Salmonella typhimurium* AhpC [30], and 6.6 in *Mycobacterium tuberculosis* AhpE [31], and given the hydrogen bond network around Cys51-SO^-, the Cys51 Tpx-B sulfenic acid is expected to be in its sulfenate form (RSO^-) under physiological conditions.

The effect of the Tyr43Ala, Val50Ala, Arg127Ala and Thr48Ala mutation on the sulfenic acid/thiol reduction potential was calculated via (9). The value of $\Delta G°'(RSO^- / RS^-)$ in the Arg127Ala and the Thr48Ala mutants was found to be decreased compared to wild type by 22 kcal/mol and 4 kcal/mol respectively (Table 3). The polar residues Arg127 and Thr48 thus favor the Cys51 oxidation. Both effects are significant according to the correlation curve presented in Figure 2. The effect of the non-polar residues Val50 and Tyr43 was found to be insignificantly small. Using the first version of the REE method and a different model system of the Prx active site, the non-polar residue Val was found to favor thiol sulfenylation with 4 kcal/mol[8], while the other non-polar residue tested, Trp86 disfavors oxidation by 2 kcal/mol[8]. These results are not dependent on the version of the REE method (first version from ref.[8] or updated, presented here), but on the model system. Therefore, a QM/MM approach on the entire protein is applied in the next section to obtain data that are not model system dependent and that include protein dynamics (cfr. several snapshots from a molecular dynamics run were analyzed, see further).

Factors that control the Cys51 oxidation in human Prx: results from QM/MM calculations-Part1: Hydrogen bonds in QM/MM optimized structures

13 snapshots were taken from the 5ns molecular dynamics (MD) run and QM/MM optimized (see Methods section) to use in the REE analysis. The QM part of the QM/MM system is exactly the same as in the QM only calculations discussed in the previous section (Figure 4). For convenience, these structures are called the QM/MM structures throughout the further discussion.

The hydrogen bond pattern found in the QM/MM optimized structures differs from that found in the QM structures (Table 4, Figure 4).

Figure 4: Interactions between Cys51-S^- (**A**) and Cys51-SO^- (**B**) in the QM/MM optimized structures of Tpx-B. See Table 4 for the interaction distances. Color code: nitrogen: blue; oxygen: red; hydrogen: white; carbon: green, sulfur: yellow. This figure was generated using Pymol [11].

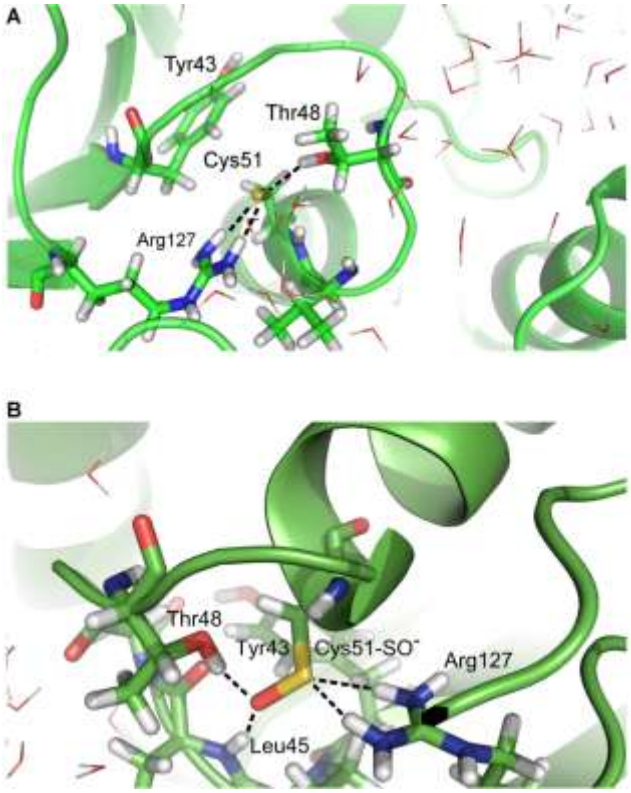

In the reduced wild type (WT) structure, three permanent hydrogen bonds are present: Thr48OγH--Cys51S^-, Arg127Nη_1H--Cys51S^- and Arg127Nη_2H--Cys51S^-. The hydrogen bond with Thr48 is not present in the QM structures (Table 2, Figure 3). In the oxidized form of the WT structure, Cys51-SO^- forms two hydrogen bonds with Arg127 and one with the OH

group of Thr48 and another one with the backbone amide group of Leu45, which replaces the hydrogen bond between the backbone NH of Cys51 $NH_{backboneCys51}$--Cys51SO^- observed in the oxidized QM structures. In the snapshots from the MD trajectory of the oxidized form, the hydrogen bond between $NH_{backboneCys51}$--Cys51(O) is present, however in the course of the QM/MM optimization rotation around the Cβ-S bond led to the formation of the $NH_{backboneLeu45}$ --Cys51(O) hydrogen bond and the disappearance of the $NH_{backboneCys51}$--Cys51(O) hydrogen bond. Arg127 interacts mainly with the S atom of $–SO^-$ in the oxidized active site of the QM/MM structures (Figure 4), while in the QM structures, Arg127 interacts equally with both the S and O atoms. Further, in comparison to the QM structures, Tyr43 shifts to the oxygen atom of $–SO^-$ in the QM/MM optimized structures (Figure 4, Table 4).

In both the oxidized and the reduced forms, in general one water molecule forms a transient hydrogen bond to Cys51 (Figure 5).

Figure 5: Spatial distribution of the fast interchanging water molecules in the QM/MM optimized structures of wild type Tpx-B in the Cys51-S^- (**A**) and Cys51-SO^- (**B**) form. See Table 4 for the interaction distances. Color code: nitrogen: blue; oxygen: red; hydrogen: white; carbon: green, sulfur: yellow. This figure was generated using Pymol [11].

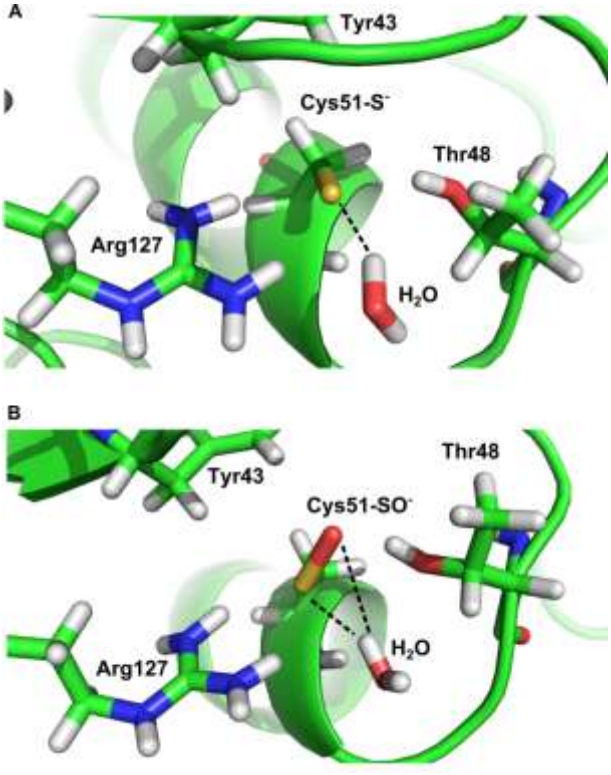

This water molecule is rapidly changing throughout the MD run indicating the very weak character of the interaction, and therefore it was not included in the QM region of the QM/MM set up (see next paragraph). The fast interchange of water molecules is facilitated by the extended water channel (Figure 6) leading up from the bulk water to Cys51. Most likely this solvent channel allows also for the easy access of oxidizing agents to the reactive Cys51 residue.

Figure 6: The water channel, represented in stick representation, provides a route to the bulk solvent by which the water molecules can fast interchange and thus interact only transiently with Cys51-S^- and Cys51-SO^-. See Table 4 for the interaction distances. Color code: nitrogen: blue; oxygen: red; hydrogen: white; carbon: green, sulfur: yellow. This figure was generated using Pymol [11].

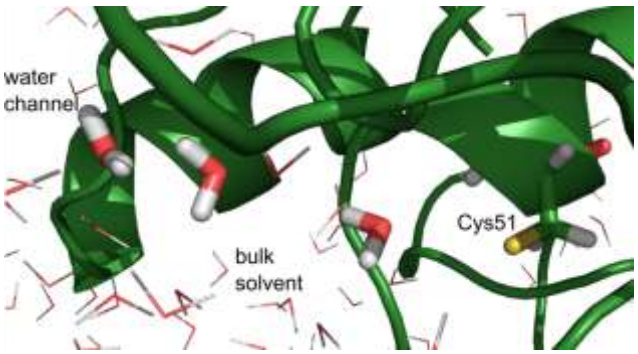

In the QM/MM optimized structures of the Arg127Ala mutant, the hydrogen bond network around Cys51-S^- is broken. Basically, Cys51-S^- interacts only with two or three water molecules that are continuously present on hydrogen bonding distance from Cys51 and take the position of the Arg127 guanidinium group (Figure 7). This is also seen in the oxidized form of the Arg127Ala mutant in which Cys51-SO^- forms almost exclusively hydrogen bonds with three to four water molecules.

In the other mutants, the hydrogen bond interactions found in the WT structure are in general preserved (see Table 4 for details).

Figure 7: Two water molecules take the position of the Arg127 guanidinium group in the QM/MM optimized structure of the Arg127Ala mutant (green: wild type, cyan: Arg127Ala). For interaction distances, see Table 4. Color code: nitrogen: blue; oxygen: red; hydrogen: white, sulfur: yellow. This figure was generated using Pymol [11].

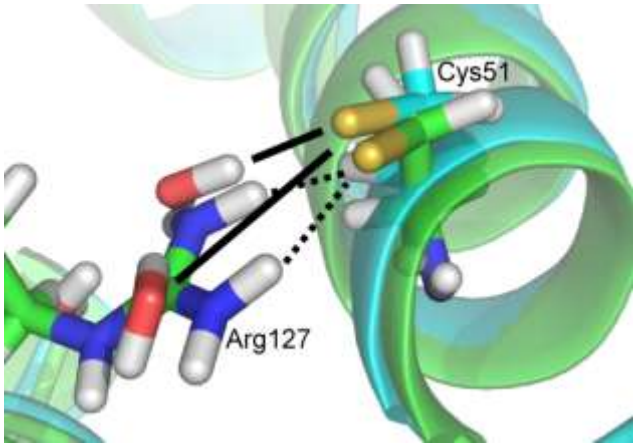

Factors that control the Cys51 oxidation in human Prx: results from QM/MM calculations-Part2: Sulfenylation thermodynamics

To obtain reliable and comparable energies, a single point calculation on the QM region of the QM/MM optimized structures is performed (Table 5) in a continuous solvent model (see Methods section). The QM region and the solvent model are exactly the same as for the QM structures discussed in a previous section.

The difference in hydrogen bonding pattern between the QM and QM/MM structures has consequences for the effect on the sulfenylation thermodynamics (Table 5).

The most striking difference is seen for Arg127. From the calculation of $\Delta\Delta G°'(RSO^{-} / RS^{-})$ according to the REE methodology on the QM/MM structures, it can be seen that Arg127 disfavors the sulfenylation with ~16 kcal/mol. For the QM structures, we found that Arg127 favors sulfenylation with ~20kcal/mol. This difference can be explained via the results from model calculations in Table 1. From these calculations it can be seen that

cationic groups slightly disfavor sulfenylation when they interact with the oxygen of the SO^- form. However, it is expected (Scheme 2) that they increasingly disfavor sulfenylation when they would interact with the sulfur of SO^- group due to the much less favorable electrostatic attraction between the groups, as sulfur is much less negatively charged than oxygen in SO^- (in CH_3SO^- the Mulliken charge calculated at the B3LYP/6-31+G(d,p) level on the S atom is -0.12 and -0.85 on the oxygen atom). In the QM/MM geometry, Arg127 mainly interacts with the S atom of $–SO^-$ and thus exerts a much more unfavorable effect than in the QM geometry in which Arg127 interacts equally with both the O and S atom. Further, water molecules take over the place of Arg127 in the QM/MM structures, which is not the case in the QM structures (because these structures were not solvated before optimization). The model calculations (Table 1) shows that polar ligands favor the sulfenylation reaction, and thus, the appearance of these ligands favor sulfenylation in the Arg127Ala mutant. The water molecules can repair and even reverse the effect of mutating Arg127 to Ala compared to the QM structures, in which no water molecules are present to take over the role of Arg127. In order to prove this hypothesis, we have deleted the water molecules from the QM/MM structures of the Arg127Ala mutant and recalculated the energy. Based on these calculations the REE model suggests indeed that Arg127 favors sulfenylation, similarly to the QM calculations, although to a lower extent with ~5kcal/mol.

Although water molecules seem to enhance the easiness of sulfenylation of Cys51 in the Arg127 mutant, it is still likely that Arg127 play an important role in stabilizing the position of the cysteine thiolate side chain and allowing the sulfenylation reaction to proceed more easily. However, based on p*K*a calculations on the QM/MM structures via the natural population analysis charge-p*K*a correlation method presented elsewhere [28], we found a p*K*a of Cys51 in the Arg127Ala mutant of 5.4, which is similar to the p*K*a in the wild type, which is calculated to be 5.7.

Kinetic experiments with Arg127 mutated to Lys show that the rate constant drops with a factor 5 [12]. Perhaps here, when Lys is present in the position of Arg, it cannot fix the cysteine thiolate side chain in a position optimal for the reaction with H_2O_2 in the same way as the guanidinium group of Arg does. When Lys is present there might be no room for water molecules to come in to take over the interaction missing in the absence of Arg. However, it should also be kept in mind that thermodynamic and kinetic factors might not always show the same trend.

Based on the QM/MM structures, Thr48 favors sulfenylation, in agreement with the findings on the QM only structures. Based on the presence of the Thr48OγH--Cys51 interaction with the O atom of $–SO^-$ in the wild type structure (Table 5), one can expect that in the Thr48Ala the SO^- form is destabilized compared to the wild type as in this mutant, the crucial Thr48OγH--Cys51 hydrogen bond interaction is no longer present. This is in agreement with the calculated ligand effects on small models systems (Table 1) and with thermodynamic cycle depicted in Scheme 2. The active site Thr has also a positive effect on sulfenylation kinetics [13] [14] and thus for this residue, kinetic and thermodynamic factors show the same trend.

Further, the QM/MM structures reveal that the Tyr43Ala mutation disfavors sulfenylation with ~9 kcal/mol suggesting that Tyr43 favors sulfenylation. For the QM only structures, no effect of Tyr43 was found. As was discussed in connection to Scheme 2, the effect of a given side chain on the sulfenylation reaction originates from the fact that it interacts differently with the S^- and SO^- forms of cysteine compared to wild type. The sulfenylation reaction can become more favored either by destabilizing the S^- form compared to the wild type or by stabilizing the SO^- form compared to the wild type. Based on the QM/MM structures, in the Tyr43Ala mutation, the S^- form becomes stabilized compared to the wild type as more hydrogen bonds are made to the S^- form in the Tyr43Ala mutation than in the WT type, while in the SO^- form the same number (4) of hydrogen bonds are made to the protein (Table 4). This difference in hydrogen bond pattern between mutant and wild type is not found in the QM only structures (Table 3).

The effect of Val50 obtained from both the QM/MM and the QM structures is small. This is in agreement with the absence of interactions between Val50 and Cys51.

To give a more support to our conclusions, we have estimated the SO bond enthalpy in the various mutants as a measure of the reactivity of thiolate group in the various mutants. The accurate calculation of bond enthalpies in many-atom systems is not straight-forward due to the need to sample many different structures of the bonded system and the fragments [32], but a similar approach has already been used to compare the reactivities of the oxidizing species of various cytochrome P450 enzymes [33]. The thermodynamic cycle depicted in Scheme 3 shows the relationship between the S-O bond enthalpy and the overall reaction energy of the sulfenylation reaction.

The overall reaction energy, ΔE_{S-O} can be calculated as

$$\Delta E_{S-O} = \Delta E_1 + \Delta E_2 \qquad (12)$$

where ΔE_1 is the energy required to break the peroxide bond and form water and an oxygen atom. This term is considered as constant for the studied systems in the first approximation assuming that the solvation of H_2O_2 is the same in all active sites. ΔE_2 is the energy released upon addition of an oxygen atom to cysteine sulfide. This term is independent of the oxidizing species and fundamentally influence the exothermicity of the overall reaction. The negative of ΔE_2 is the S-O bond enthalpy. Smaller values of ΔE_2 correspond to weaker -S-O bonds and thus less exothermic scavenging reactions. Therefore mutations which increase the value of ΔE_2 will favor sulfenylation (i.e. the originally mutated residue will disfavour sulfenylation).

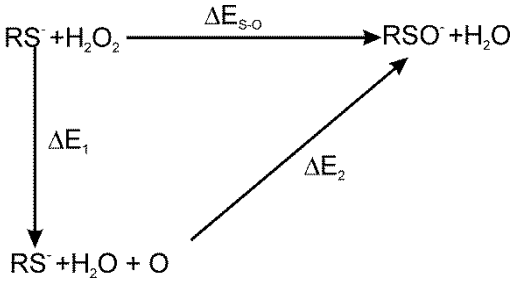

Scheme 3: Thermodynamic cycle showing the importance of the S-O bond enthalpy

The calculated bond enthalpies (Table 5) show significant changes over the various mutants. The standard deviation of the bond enthalpies is relatively small and indicates that the observed effects are indeed significant. The Thr48Ala and Tyr43Ala mutants have a smaller bond enthalpy than the wild type, while the Arg127Ala mutant has a larger bond enthalpy. This indicates that Thr48 and Tyr43 favor oxidation, while Arg127 thermodynamically disfavor oxidation, in accordance with the conclusions based on the REE model.

Conclusion

In conclusion, compared to the QM only calculations, the QM/MM calculations give a completely new insight into sulfenylation thermodynamics. Comparison with experimentally obtained redox potentials would strengthen our results. However, the experimental validation of the REE method not possible. Instead, the results obtained using the REE methodology on the QM/MM optimized structures could be validated from insights obtained from free energy calculations on small model systems. Based on the REE methodology, which can be universally applied to other systems, we could unravel the effects of several residues on the thiol/sulfenic acid oxidation potential of human Tpx-B. The effect of these residues could be linked to the hydrogen bond pattern found in the QM/MM optimized structures, relating structure to reactivity. The hydrophobic Tyr43 residue together with Arg127 and Thr48 might create the optimum circumstances for thiol oxidation in the active site cavity. It provides enough reactivity for sulfenylation to happen, but it is not too reactive in order to prevent fast and immediate over-oxidation to sulfonic acid. This subtle interplay between polar and non-polar active site residues makes human Tpx-B an efficient ROS scavenger.

Acknowledgements

The authors thank Jeremy Harvey (University of Bristol) for useful discussions. JO acknowledges the financial support of a EU Marie Curie ERG Fellowship (Project "Oestrometab"), of a Bolyai János Research Fellowship and of the New Széchenyi Plan (TÁMOP-4.2.2/B-10/1-2010-0009). GR thanks the FWO for a post doctoral fellowship. GR, FDP and LvB wish to acknowledge financial support of the Research Foundation Flanders (FWO) through research program FWOAL622.

Table 1: Relative effect of polar and non-polar ligands on the reaction free energy $\Delta G°'(RSO^- / RS^-)$ (in kcal/mol) of the CH_3SO^---L → CH_3S^---L reduction calculated as $\Delta\Delta G°'(RSO^- / RS^-)_{ref-ligand} = \Delta G°'_{ref} - \Delta G°'_{ligand}$. The indicated calculation levels give the level at which the structures are optimized and thus the level of the gas phase free energies of Eq. (1). The free energies of solvation are calculated using the PCM model [16], with UAHF radii in aqueous solution calculated at the HF/6-31+G(d) level[15b].

Ligand type	Ligand	B3LYP/6-31+G(d,p)		M06-2X/6-31+G(d,p)		MP2/6-31+G(d,p)		MP2/6-311++G(d,p)	
		Interacting site of the CH_3SO^- molecule							
		O	S	O	S	O	S	O	S
	None (Reference)	0.0		0.0		0.0		0.0	
polar	CH_3OH	-2.2	ND*	-4.5	ND	-3.1	ND*	-2.1	ND*
	H_2O	-3.1	ND*	-5.0	ND*	-3.5	ND*	-3.3	ND*
	NH_3	-0.6	ND*	-1.6	-0.7	-1.6	-1.0	-1.2	-0.5
	CH_3COOH	ND**	5.8	ND**	4.5	ND**	3.4	ND**	7.6
	CH_3CONH_2	-2.6	ND*	-4.1	ND*	-3.5	ND*	-2.7	ND*
Cation	Na+	1.9	ND*	ND$	ND$	1.6	ND*	2.0	ND*
Non-polar	CH_4	4.3	0.0	2.3	-0.1	3.0	0.2	4.3	0.35
	C_2H_4	3.7	ND*	2.6	ND*	2.8	ND*	4.3	ND*
	benzene	3.4		1.2		4.2		5.8	

ND: not determined; **proton transfer to SO^-; *the ligand redirects to oxygen; $Structures having imaginary frequencies

Table 2: Hydrogen bonds around $Cys51S^-$ and $Cys51SO^-$ obtained in the optimized geometries of the models (QM structures) of the active site around Cys51. Hydrogen bonds are interactions formed between a donor group (D−H) and an acceptor atom (A), resulting in the pattern: $D^{\delta-}–H^{\delta+}---A^{(\delta)-}$. Distances (in Å) are measured between H and A, except for Tyr, where the distance between D and A is measured.

	WT		Arg127Ala		Thr48Ala		Tyr43Ala		Val50Ala	
	$Cys51S^-$	$Cys51SO^-$	$Cys51S^-$	$Cys51SO^-$	$Cys51S^-$	$Cys51SO^-$	$Cys51S^-$	$Cys51SO^-$	$Cys51S^-$	$Cys51SO^-$
Arg127Nη_1H--Cys51	2.13	1.76 (O)*	NA	NA	2.21	1.64 (O)	2.56	1.74 (O)	2.13	1.74 (O)
Arg127Nη_2H--Cys51	2.57	2.28 (S)	NA	NA	2.59	2.35 (S)	2.12	2.28 (S)	2.57	2.27 (S)
H_2O--Cys51	3.18	1.71 (O)	2.15	1.61 (O)	3.12	1.72 (O)	3.18	1.71(O)	3.18	1.71 (O)
Thr48OγH--Cys51	NA	2.11 (O)	2.27	1.57 (O)	NA	NA	NA	2.14 (O)	NA	2.12 (O)
$NH_{backboneCys51}$--Cys51	NA	2.09 (O)	NA	1.93 (O)	NA	1.95(O)	NA	2.06 (O)	NA	2.09 (O)
Tyr43----Cys51[a]	4.09	3.86 (S)	4.60	3.93 (S)	4.13	3.90 (S)	NA	NA	4.09	3.86 (S)

[a] Distance towards C-atom of the phenol group that is closest to the Cys51 sulfur . NA: not applicable

* (O) or (S) indicates that an interaction with the oxygen/sulfur atom of the sulfenic acid is formed.

Table3: $\Delta\Delta G^{\circ\prime}(RSO^{-}/RS^{-})_{\text{WT-mutant}}$ (in kcal/mol) of different mutants calculated relatively to the WT structure in kcal/mol. $\Delta\Delta E(RSO^{-}/RS^{-})$ was calculated on the QM model system of the active site and can be directly linked to reduction potential differences via $\Delta\Delta G^{\circ\prime}(RSO^{-}/RS^{-})_{\text{WT-mutant}} = C\Delta E(RSO^{-}/RS^{-})_{\text{WT}} - C\Delta E(RSO^{-}/RS^{-})_{\text{mutant}}$ with C=0.99 (Figure 2).

	$\Delta\Delta G^{\circ\prime}(RSO^{-}/RS^{-})_{\text{WT-mutant}}$
WT	0.0 (ref)
Arg127Ala	21.9
Thr48Ala	3.7
Tyr43Ala	-0.4
Val50Ala	-0.4

Table 4: Hydrogen bonds around $Cys51S^-$ and $Cys51SO^-$ obtained in the QM/MM optimized geometries. Hydrogen bonds are interactions formed between a donor group (D−H) and an acceptor atom (A), resulting in the pattern: $D^{\delta-}–H^{\delta+}---A^{(\delta)-}$. Distances (in Å) are measured between H and A, except for Tyr, where the distance between D and A is measured.

	WT		Arg127Ala		Thr48Ala		Tyr43Ala		Val50Ala	
	$Cys51S^-$	$Cys51SO^-$	$Cys51S^-$	$Cys51SO^-$	$Cys51S^-$	$Cys51SO^-$	$Cys51S^-$	$Cys51SO^-$	$Cys51S^-$	$Cys51SO^-$
Arg127Nη_1H--Cys51	2.267±0.050	3.510±0.143 (O) 2.479±0.103 (S)	NA	NA	2.426±0.125	3.509±0.268 (O) 2.642±0.183 (S)	2.396±0.076	3.611±0.136 (O) 2.673±0.178 (S)	2.353±0.054	3.570±0.104 (O) 2.302±0.073 (S)
Arg127Nη_2H--Cys51	2.314±0.038	3.513±0.059 (O) 2.265±0.026 (S)	NA	NA	2.288±0.062	3.286±0.104 (O) 2.191±0.025 (S)	2.311±0.060	3.451±0.201 (O) 2.275±0.073 (S)	2.279±0.030	3.509±0.182 (O) 2.444±0.122 (S)

H_2O--Cys51[c]	2.367 ±0.104	2.437±0.171(S)	2.219±0.053	2.409±0.072 (S)[d]	2.299±0.062	2.372±0.314 (S)	2.472±0.096	2.580±0.225(S)	2.383±0.059	2.434±0.156 (S)
		1.669±0.042(O)	2.288±0.065	1.456±0.097 (O)[d]		1.666±0.043 (O)		1.686±0.050 (O)		1.709±0.037
				1.936±0.395 (O)[d]						
average number of H-bonds from water[b]	0.769	1.077 (S)	2.308	3.231(S)	0.923	1.385(S)	0.538	1.538(S)	0.846	1.000(S)
		0.538(O)		2.077(O)		0.615(O)		0.923(O)		0.769(O)
Thr48OγH--Cys51	2.381±0.176	1.883±0.310 (O)	3.206±0.294	3.072±0.431(O)	NA	NA	2.357±0.262	2.151±0.563 (O)	3.162±0.324	1.739±0.054 (O)
		2.727±0.289 (S)		3.346±0.279(S)				2.768±0.418(S)		2.630±0.059 (S)

Tyr43----Cys51[a]	4.180	4.314±0.128 (S)	4.237±0.290	5.125±0.280(S)	4.375±0.321	4.476±0.193 (S)	NA	NA	4.376±0.246	4.386±0.185 (S)
		3.848±0.235 (O)		4.322±0.442 (O)		4.004 (O) ±0.461				3.960±0.206 (O)
$NH_{backboneLeu45}$--Cys51		2.363±0.238 (O)		3.410±0.498 (O)		2.062±0.163 (O)		2.025±0.112 (O)		2.483±0.222 (O)

[a] Distance towards C-atom of the phenol group that is closest to the Cys51 sulfur

[b] The average number of hydrogen bonds towards the S or O atom of the Cys51 sulfur has been calculated by summing the number of short H_{wat}-S or H_{wat}-O distances over all snapshots and divided by the number of snapshots (13) for a given system

[c] In the case of the Arg127Ala mutant systems three water molecules close to the Cys51 sulfur were included in the QM/MM optimization process. In the case of all other systems all water molecules were described by an MM model.

[d] Distances to Cys51 were measured only from quantum mechanically described water molecules.

* (O) or (S) indicates that an interaction with the oxygen/sulfur atom of the sulfenic acid is formed.

NA: not applicable

Table5: ΔE_{S-O} and $\Delta E(RSO^- / RS^-)$ calculated on the QM/MM systems. $\Delta E(RSO^- / RS^-)$ is calculated according to equation (6), in which $E(H_2O)$ is included as a constant contribution. $\Delta\Delta G^{\circ\prime}(RSO^- / RS^-)_{\text{WT-mutant}}$ of different mutants calculated relatively to the WT structure. $\Delta\Delta E(RSO^- / RS^-)$ can be directly linked to reduction potential differences via $\Delta\Delta G^{\circ\prime}(RSO^- / RS^-)_{\text{WT-mutant}} = C\Delta E(RSO^- / RS^-)_{\text{WT}} - C\Delta E(RSO^- / RS^-)_{\text{mutant}}$ with C=0.99 (Figure 2). All standard deviations are obtained by error propagation. All values are given in kcal/mol.

	ΔE_{S-O}	$\Delta E(RSO^- / RS^-)$	$\Delta\Delta G^{\circ\prime}(RSO^- / RS^-)_{\text{WT-mutant}}$
WT	76.7±4.58	-47182.7±4.58	0.0 (ref)
Arg127Ala	92.6±6.29	-47198.6±6.29	-15.5
Arg127Ala (no water)	71.3±5.63	-47177.3±5.63	5.30
Thr48Ala	66.5±2.88	-47172.4±2.88	10.1
Tyr43Ala	67.5±6.46	-47173.5±6.46	9.0
Val50Ala	78.8±3.29	-47184.8±3.29	-2.1

Supporting Information for:

How does the protein environment optimize the thermodynamics of thiol sulfenylation: insights from model systems to QM/MM calculations on human 2-Cys peroxiredoxin?

Table S1:

Protocol S1:

Table S1: Interaction energies, calculated using basis set suppperposition error correction at the MP2/6-31++G(d,p) level, between ligand L and CH_3S^- and CH_3SO^- in the CH_3S^- --L and CH_3SO^---L complexes optimized at the B3LYP/6-31+G(d,p) level. Values are given in kcal/mol.

L	CH3S-	CH3SO-	
		L interacts with S	L interacts with S
CH_4	-1.9	-0.9	-3.3
H_2O	-14.8	ND	-21.0
CH_3COOH	-33.1	-28.0	ND

Topology file and added parameters for deprotonated cystein (Cys-S-) and oxidized cystein (Cys-SO-)

Topology file:

New atom types for oxidized cystein:

```
MASS   288 SZ    32.06000 S ! sulfur of oxidized CYS
MASS   289 OZ    15.99900 O ! oxygen of oxidized

PRES DCY        -1.00  ! patch residue used to make deprotonated cystein (CysS-)
DELETE ATOM HG1
GROUP
ATOM CB   CT2    -0.38
ATOM HB1  HA      0.09
ATOM HB2  HA      0.09
ATOM SG   SS     -0.80

PRES CSO     -1.00  ! patch for oxidized CYS with negative charge. (Cys-SO-)
DELETE ATOM HG1
GROUP
ATOM CB   CT2   -0.33  !
ATOM HB1  HA     0.11  !
ATOM HB2  HA     0.11  !
ATOM SG   SZ    -0.13  !
ATOM OE   OZ    -0.76  !
BOND  SG OE
ACCEPTOR OE SG
BILD CA   CB   SG   OE    1.5584 113.8700 180.0000 103.9700  1.6038
END
```

Parameters

The parameters were either obtained by analogy, in this case the comment shows the origin of the parameters. In the case of Cys-SO- the parameters were obtained by studying CH_3-SO- at the MP2/6-311++G** level and fitting the MM parameters to the QM potential energy surface.

BONDS

```
SS   CT2    205.000     1.8360 ! added by JO. as SS-CS: methylthiolate 6-31+G* i
NH2   CT1   240.00      1.455  ! From LSN NH2-CT2
SZ   CT2   198.000     1.8180 ! Equal to S CT2 parameter
SZ   OZ    295.000     1.6038 ! added for oxidated CYS based on CH3-SO(-) MP2/6-
311++G** geom/freq
```

ANGLES

SS CT2 CT1 58.000 112.5000 ! based on CT1-CT2-S from normal cysteine
SS CT2 HA 46.100 111.3000 ! based on CT1-CT2-S from normal cysteine
SZ CT2 CT1 58.000 114.500 ! Equal to S-CT2-CT1 parameter
SZ CT2 HA 46.100 111.300 ! Equal to S-CT2-HA parameter
CT2 SZ OZ 56.0 104.000 ! added for oxidized CYS system based on the CH3CH2SO(-) MP2/6-311++G** geom/freq calculation

DIHEDRALS

CT1 CT2 SZ OZ 1.2000 2 180.00 ! based on CH3CH2SO (-) MP2/6-311++G** calculation
CT1 CT2 SZ OZ 1.7500 3 180.00 ! based on CH3CH2SO (-) MP2/6-311++G**
HA CT2 SZ OZ 1.6500 3 180.00 ! based on CH3CH2SO (-) MP2/6-311++G**

NONBONDED

SZ 0.000000 -0.450000 2.000000 ! ox. CYS system
! LVB 24/01/13
OZ 0.000000 -0.120000 1.700000 0.000000 -0.120000 1.400000 ! ox. CYS system
!

References:

[1] Z. A. Wood, E. Schroder, J. Robin Harris and L. B. Poole, *Trends Biochem. Sci.* **2003**, *28*, 32-40.
[2] L. B. Poole, *Subcell. Biochem.* **2007**, *44*, 61-81.
[3] L. Flohe, *Methods in Enzymology, Vol 473: Thiol Redox Transitions in Cell Signaling, Pt A: Chemistry and Biochemistry of Low Molecular Weight and Protein Thiols* **2010**, *473*, 1-39.
[4] G. Roos, Messens, J., *Free Radic. Biol. Med.* **2011**, *51*, 314-326.
[5] a) C. C. Winterbourn and M. B. Hampton, *Free Radical Biology and Medicine* **2008**, *45*, 549-561; b) M. C. Trujillo, A.; Manta, B.; Ferrer-Sueta, G.; Smeets, A.; Declercq, J. P.; Knoops, B.; Radi, R., *Arch. Biochem. Biophys.* **2007**, *467*, 95-106; c) H. Budde, L. Flohe, H. J. Hecht, B. Hofmann, M. Stehr, J. Wissing and H. Lunsdorf, *Biol. Chem.* **2003**, *384*, 619-633; d) D. Parsonage, D. S. Youngblood, G. N. Sarma, Z. A. Wood, P. A. Karplus and L. B. Poole, *Biochemistry* **2005**, *44*, 10583-10592; e) A. V. Peskin, F. M. Low, L. N. Paton, G. J. Maghzal, M. B. Hampton and C. C. Winterbourn, *J. Biol. Chem.* **2007**, *282*, 11885-11892; f) A. G. Cox, C. C. Winterbourn and M. B. Hampton, *Biochem. J.* **2010**, *425*, 313-325.
[6] G. Ferrer-Sueta, B. Manta, H. Botti, R. Radi, M. Trujillo and A. Denicola, *Chem. Res. Toxicol.* **2011**, *24*, 434-453.
[7] L. B. Poole, P. A. Karplus and A. Claiborne, *Annu. Rev. Pharmacol. Toxicol.* **2004**, *44*, 325-347.
[8] L. Billiet, P. Geerlings, J. Messens and G. Roos, *Free Radic. Biol. Med.* **2012**, *52*, 1473-1485.
[9] A. Hall, P. A. Karplus and L. B. Poole, *FEBS J* **2009**, *276*, 2469-2477.
[10] E. Schroder, J. A. Littlechild, A. A. Lebedev, N. Errington, A. A. Vagin and M. N. Isupov, *Struct. Fold. Des.* **2000**, *8*, 605-615.
[11] in *The PyMOL Molecular Graphics System Version 1.5.0.4, Vol.* Schrödinger, LLC.
[12] P. Nagy, A. Karton, A. Betz, A. V. Peskin, P. Pace, R. J. O'Reilly, M. B. Hampton, L. Radom and C. C. Winterbourn, *J. Biol. Chem.* **2011**, *286*, 18048-18055.
[13] L. Flohe, H. Budde, K. Bruns, H. Castro, J. Clos, B. Hofmann, S. Kansal-Kalavar, D. Krumme, U. Menge, K. Plank-Schumacher, H. Sztajer, J. Wissing, C. Wylegalla and H. J. Hecht, *Arch. Biochem. Biophys.* **2002**, *400*, 148-148.
[14] P. Lamkemeyer, M. Laxa, V. Collin, W. Li, I. Finkemeier, M. A. Schottler, V. Holtkamp, V. B. Tognetti, E. Issakidis-Bourguet, A. Kandlbinder, E. Weis, M. Miginiac-Maslow and K. J. Dietz, *Plant J.* **2006**, *45*, 968-981.
[15] a) J. M. Ho and M. L. Coote, *Theor. Chem. Acc.* **2010**, *125*, 3-21; b) J. Ho, A. Klamt and M. L. Coote, *J. Phys. Chem. A* **2010**, *114*, 13442-13444.
[16] J. Tomasi, B. Mennucci and R. Cammi, *Chem. Rev.* **2005**, *105*, 2999-3093.
[17] J. Ho, M. L. Coote, C. J. Cramer and D. G. Truhlar in *Theoretical Calculation of Reduction Potentials, Vol.* Eds.: B. Speiser and O. Hammerich), CRC Press, Boca Raton, FL, **2012, in press**.
[18] G. W. T. M. J. Frisch, H. B. Schlegel, G. E. Scuceria, M. A. Robb, J. R. Cheeseman, J. A. Montgomery, Jr., T. Vreven, K. N. Kudin, J. C. Burant, J. M. Millam, S. S. Iyengar, J. Tomasi, V. Barone, B. Mennucci, M. Cossi, G. Scalmani, N. Rega, G. A. Petersson, H. Nakatsuji, M Hada, M. Ehara, k. Toyota, R. Fukuda, J. Hasegawa M. Ishida, T. nakajima, Y. Honda, O. Kitao, H. Nakai, M. Klene, X. Li, J. E. Knox, H. P. Hratchian, J. B. Cross, C. Adamo, J. Jaramillo, R. Gomperts, R. E. Stratmann, O. Yazyev, A. J. Austin, R. Cammi, C.

Pomelli, J. W. Ochterski, P. Y. Ayala, K. Morokuma, G. A. Voth, P. Salvador, J. J. Dannenberg, V. G. Zakrzewski, S. Dapprich, A. D. Daniels, M. C. Strain, O. Farkas, D. K. Malick, A. D. Rabuck, K. Raghavachari, J. B. Foresman, J. V. Ortiz, Q. Cui, A. G. Baboul, S. Clifford, J. Cioslowski, B. B. Stefanov, G. Liu, A. Liashenko, P. Piskorz, I. Komaromi, D. J. Fox, T. Keith, M. A. Al-Laham, C. Y. Peng, A. Nanayakkara, M. Challacombe, P. M. W. Gill, B. Johnson, W. Chen, M. W. Wong, C. Gonzalez, and J.A. Pople in *Gaussian 03, Revision A.1*, *Vol.* Gaussian, Inc., **2003**.
[19] G. W. T. M. J. Frisch, H. B. Schlegel, G. E. Scuseria, M. A. Robb, J. R. Cheeseman, G. Scalmani, V. Barone, B. Mennucci, G. A. Petersson, H. Nakatsuji, M. Caricato, X. Li, H. P. Hratchian, A. F. Izmaylov, J. Bloino, G. Zheng, J. L. Sonnenberg, M. Hada, M. Ehara, K. Toyota, R. Fukuda, J. Hasegawa, M. Ishida, T. Nakajima, Y. Honda, O. Kitao, H. Nakai, T. Vreven, J. A. Montgomery, Jr., J. E. Peralta, F. Ogliaro, M. Bearpark, J. J. Heyd, E. Brothers, K. N. Kudin, V. N. Staroverov, R. Kobayashi, J. Normand, K. Raghavachari, A. Rendell, J. C. Burant, S. S. Iyengar, J. Tomasi, M. Cossi, N. Rega, J. M. Millam, M. Klene, J. E. Knox, J. B. Cross, V. Bakken, C. Adamo, J. Jaramillo, R. Gomperts, R. E. Stratmann, O. Yazyev, A. J. Austin, R. Cammi, C. Pomelli, J. W. Ochterski, R. L. Martin, K. Morokuma, V. G. Zakrzewski, G. A. Voth, P. Salvador, J. J. Dannenberg, S. Dapprich, A. D. Daniels, Ö. Farkas, J. B. Foresman, J. V. Ortiz, J. Cioslowski, and D. J. Fox in *Gaussian 09, Revision A.1*, *Vol.* Gaussian, Inc., Wallingford CT, **2009**.
[20] M. H. Olsson, C. R. Søndergard, M. Rostkowski and J. H. Jensen, *J. Chem. Theory Comput.* **2011**, *7*, 525-537.
[21] M. W. van der Kamp in *PhD thesis, Modelling reactions and dynamics of Claisen enzymes, Chapter 4.6, Vol.* University Bristol, **2008**.
[22] A. D. MacKerell, Jr., N. Banavali and N. Foloppe, *Biopolymers* **2000**, *56*, 257-265.
[23] B. R. Brooks, C. L. Brooks, 3rd, A. D. Mackerell, Jr., L. Nilsson, R. J. Petrella, B. Roux, Y. Won, G. Archontis, C. Bartels, S. Boresch, A. Caflisch, L. Caves, Q. Cui, A. R. Dinner, M. Feig, S. Fischer, J. Gao, M. Hodoscek, W. Im, K. Kuczera, T. Lazaridis, J. Ma, V. Ovchinnikov, E. Paci, R. W. Pastor, C. B. Post, J. Z. Pu, M. Schaefer, B. Tidor, R. M. Venable, H. L. Woodcock, X. Wu, W. Yang, D. M. York and M. Karplus, *J. Comp. Chem.* **2009**, *30*, 1545-1614.
[24] a) N. Foloppe, J. Sagemark, K. Nordstrand, K. D. Berndt and L. Nilsson, *J. Mol. Biol.* **2001**, *310*, 449-470; b) N. Foloppe and L. Nilsson, *Structure* **2004**, *12*, 289-300.
[25] K. Vanommeslaeghe, E. Hatcher, C. Acharya, S. Kundu, S. Zhong, J. Shim, E. Darian, O. Guvench, P. Lopes, I. Vorobyov and A. D. Mackerell, Jr., *J. Comp. Chem.* **2010**, *31*, 671-690.
[26] in *ChemShell, a Computational Chemistry Shell, see www.chemshell.org, Vol.*
[27] G. Roos, N. Foloppe and J. Messens, *Antioxid Redox Signal* **2013**, *18*, 94-127.
[28] G. Roos, N. Foloppe, K. Van Laer, L. Wyns, L. Nilsson, P. Geerlings and J. Messens, *PLOS Comput. Biol.* **2009**, *5*, e1000461.
[29] P. Nagy and M. T. Ashby, *J Am Chem Soc* **2007**, *129*, 14082-14091.
[30] L. B. Poole and H. R. Ellis, *Methods Enzymol* **2002**, *348*, 122-136.
[31] M. Hugo, L. Turell, B. Manta, H. Botti, G. Monteiro, L. E. S. Netto, B. Alvarez, R. Radi and M. Trujillo, *Biochemistry* **2009**, *48*, 9416-9426.
[32] a) P. K. Sharma, Z. T. Chu, M. H. Olsson and A. Warshel, *Proc. Natl. Acad. Sci. U.S.A.* **2007**, *104*, 9661-9666; b) N. Strickland, A. J. Mulholland and J. N. Harvey, *Biophys. J.* **2006**, *90*, L27-29.
[33] R. Lonsdale, J. Olah, A. J. Mulholland and J. N. Harvey, *J. Am. Chem. Soc.* **2011**, *133*, 15464-15474.